

# Continuous-variable quantum approximate optimization on a programmable photonic quantum processor

Yutaro Enomoto,\* Keitaro Anai, Kenta Udagawa, and Shuntaro Takeda†

*Department of Applied Physics, School of Engineering, The University of Tokyo,  
7-3-1 Hongo, Bunkyo-ku, Tokyo 113-8656, Japan*

(Dated: June 16, 2022)

Variational quantum algorithms (VQAs) provide a promising approach to achieving quantum advantage for practical problems on near-term noisy intermediate-scale quantum (NISQ) devices. Thus far, intensive studies on qubit-based VQAs have been made theoretically and experimentally on several physical platforms. However, there have been much fewer theoretical proposals and no experimental implementations on continuous-variable (CV) VQAs, although CV quantum computing can process infinite-dimensional quantum information even on single-mode devices and thus has great potential in the NISQ era. Here, we implement the CV version of one of the most typical VQAs, a quantum approximate optimization algorithm, on a single-mode programmable photonic quantum computer. We experimentally demonstrate that this algorithm solves a minimization problem of a given continuous real-valued function by implementing the quantum version of gradient descent and localizing an initially broadly-distributed wavefunction to the minimum of the given function. To the best of our knowledge, this is the first demonstration ever of a practical CV quantum algorithm on any physical platform, except for Gaussian Boson sampling. Our work highlights the power of CV quantum computing in the NISQ era, opening a new door to the quantum advantage in practical problems.

Variational quantum algorithms (VQAs) have recently emerged as the leading approach to achieving quantum advantage for practical problems under the constraints of near-term noisy intermediate-scale quantum (NISQ) devices<sup>1,2</sup>. In VQAs, such constraints are avoided by the common strategy to repeatedly run shallow-depth quantum circuits with the circuit parameters updated by classical optimizers. This strategy enables us to mitigate the accumulation of errors and fully exploit the computational space offered by the limited-scale devices. Thus far, a wide variety of VQAs have been proposed theoretically for qubit-based systems, such as ones for combinatorial optimization<sup>3</sup>, chemistry simulation<sup>4</sup>, and machine learning<sup>5</sup>. They have already been demonstrated experimentally on several physical platforms<sup>4,6–10</sup>.

In contrast, there have been much fewer proposals<sup>11–15</sup> and no experimental implementations on continuous-variable (CV) VQAs, although CV quantum computing can potentially offer superior computational power in the NISQ era. The potential of CV systems lies in the ability to process infinite-dimensional quantum information even on single-mode devices, while in qubit-based systems each qubit provides only two-dimensional computational space. Furthermore, CV systems natively and efficiently handle continuous real parameters that often appear in real-world problems. In general, fully exploiting such infinite dimensionality and continuous degree of freedom in CV systems for quantum computation has been regarded as impractical due to their noise sensitivity and difficulty in error correction. However, this is in turn a promising approach to extracting high computa-

tional power in the NISQ era when the error correction is not assumed.

In this article, we implement the CV version<sup>11</sup> of one of the most typical VQAs, a quantum approximate optimization algorithm (QAOA)<sup>3</sup>, on a single-mode programmable photonic quantum computer. We experimentally demonstrate that this algorithm solves a minimization problem of a given continuous real-valued function by implementing the quantum version of gradient descent and localizing an initially broadly-distributed wavefunction to the minimum of the given function. The algorithm is shown to robustly find approximate answers to the problem with a noisy shallow-depth quantum circuit, thus confirming that the strategy of VQAs is also effective in CV systems. To the best of our knowledge, this is the first demonstration of the CV quantum algorithm designed for solving practical problems, except for Gaussian boson sampling<sup>16–18</sup>, which is designed for achieving quantum supremacy and has been partially linked to some practical problems<sup>19,20</sup>. Our work highlights the power of CV quantum computing in the NISQ era, opening a new door to the quantum advantage in practical problems.

## THEORY OF CV-QAOA

Many practical problems in various fields come down to optimization or minimization, which often require high computational costs for classical computers. The QAOA is a heuristic algorithm that could potentially offer a quantum speed-up to solve such problems on NISQ devices<sup>3</sup>. Theoretical aspects and experimental implementations of the QAOA have been recently studied intensively on qubit-based systems to solve discrete combi-

\* [yenomoto@ap.t.u-tokyo.ac.jp](mailto:yenomoto@ap.t.u-tokyo.ac.jp)

† [takeda@ap.t.u-tokyo.ac.jp](mailto:takeda@ap.t.u-tokyo.ac.jp)

natorial optimization problems<sup>6–9,21,22</sup>.

Later, a CV version of the QAOA was proposed to solve continuous optimization problems on CV systems<sup>11</sup>. This algorithm is designed for minimizations of continuous real-valued functions, which have many practical applications in finance<sup>23</sup>, machine learning<sup>24</sup>, and engineering<sup>25</sup>. This proposal<sup>11</sup> indicates that the CV-QAOA has potential of a quantum speed-up as its circuits can encode CV Grover's search algorithm<sup>26</sup>, which achieves a quadratic speed-up over the classical algorithms.

The CV-QAOA is formulated as follows. The goal of the algorithm is to find an approximate minimum of a real-valued function  $f(\mathbf{x})$  with  $\mathbf{x} = (x_1, x_2, \dots, x_N) \in \mathbb{R}^N$ . Let us consider a quantum-mechanical particle in the  $N$ -dimensional space with  $[\hat{x}_i, \hat{p}_j] = i\delta_{ij}$ , where  $(\hat{x}_1, \hat{x}_2, \dots, \hat{x}_N) = \hat{\mathbf{x}}$  and  $(\hat{p}_1, \hat{p}_2, \dots, \hat{p}_N) = \hat{\mathbf{p}}$  are position and momentum of the particle, respectively. The initial state is  $|\mathbf{p} = 0\rangle$ , which is an eigenstate of  $\hat{\mathbf{p}}$  and thus equally-weighted superposition of  $|\mathbf{x}\rangle$  for all  $\mathbf{x}$ . The unitary operator given by

$$\hat{U}(\boldsymbol{\eta}, \boldsymbol{\gamma}) = \prod_{j=1}^P e^{-i\gamma_j \hat{H}_M} e^{-i\eta_j \hat{H}_C}, \quad (1)$$

where  $\hat{H}_C = f(\hat{\mathbf{x}})$  and  $\hat{H}_M = \hat{\mathbf{p}}^2/2$ , transforms the initial state to the final state.  $P$  is the number of steps.  $\hat{H}_C$  and  $\hat{H}_M$  are called cost and mixer Hamiltonians, respectively, and  $\boldsymbol{\eta} = (\eta_1, \eta_2, \dots, \eta_P)$  and  $\boldsymbol{\gamma} = (\gamma_1, \gamma_2, \dots, \gamma_P)$  are the tunable real positive parameters. The final state is then measured in the  $\hat{\mathbf{x}}$ -basis, the measurement outcome  $\mathbf{x}$  being a candidate of the minimum of the function. This algorithm can be considered as a quantum version of the gradient descent method; a pair of the cost and mixer Hamiltonians transforms  $\hat{\mathbf{x}}$  as

$$\hat{\mathbf{x}} \rightarrow \hat{\mathbf{x}} + \gamma_j \hat{\mathbf{p}} - \eta_j \gamma_j \nabla f(\hat{\mathbf{x}}) \quad (2)$$

and indeed  $\hat{U}(\boldsymbol{\eta}, \boldsymbol{\gamma})$  represents the Trotterized approximation of the time-evolution of a particle trapped in a potential of  $f(\hat{\mathbf{x}})$  in an  $N$ -dimensional space<sup>3,11</sup>. Thus, while the distribution of  $\mathbf{x}$  is initially uniform, it moves under the influence of the potential  $f(\hat{\mathbf{x}})$  and then localizes around the minimum if the parameters  $(\boldsymbol{\eta}, \boldsymbol{\gamma})$  are properly chosen.

For the demonstration of the algorithm, we adopt the simplest problem setup, minimizing a quadratic function of one variable with the shallowest depth. Specifically, we choose  $f(x) = (x - a)^2$  with  $a \in \mathbb{R}$  ( $N = 1$ ) and set  $P = 1$ .

## PHOTONIC-CIRCUIT IMPLEMENTATION

We implement the CV-QAOA on a programmable photonic quantum computer, where optical amplitude and phase are identified with position and momentum in the algorithm, respectively. Our implementation is enabled

by recent technological advances in photonic CV quantum computing, including state preparations, gate operations, and measurements<sup>27</sup>. Especially, programmable and multi-step CV gate operations have been demonstrated very recently, which are indispensable for implementing the CV-QAOA<sup>28–30</sup>.

Our implementation can be conceptually shown in Fig. 1a. The input state is a  $p$ -squeezed state, which approximates  $|p = 0\rangle$ . After the parametrized operation of the cost and mixer on the input state, the output state is measured in the  $\hat{x}$ -basis. According to Eq. (2),  $\hat{U}(\boldsymbol{\eta}, \boldsymbol{\gamma})$  in our specific problem setting transforms  $\hat{x}$  as

$$\hat{x}_{\text{out}} = (1 - 2\eta\gamma)\hat{x}_{\text{in}} + \gamma\hat{p}_{\text{in}} + 2a\eta\gamma, \quad (3)$$

$(\hat{x}_{\text{in}}, \hat{p}_{\text{in}})$  and  $(\hat{x}_{\text{out}}, \hat{p}_{\text{out}})$  being the quadrature amplitude of the input and output states, respectively. The parameters  $\eta$  and  $\gamma$  are iteratively updated according to the sampling results of the output state.

To realize the concept of Fig. 1a, we design and implement an optical and electrical setup shown in Fig. 1b. To perform a gate operation of Eq. (3) in a programmable way, we use a measurement-induced gate composed of an ancillary state, measurement, and feedforward<sup>31</sup>. Our implementation of the gate is based on the squeezing gate in Ref. 32, from which the configuration is modified in that the beam-splitter transmissivity is made variable and the feedforward is done by classical processing. The following is a specific description of the setup. The input state is produced by an optical parametric oscillator (OPO) named OPO-1. The wavefunction of the state is squeezed in the  $p$ -direction in the sense that  $\langle \hat{x}_{\text{in}}^2 \rangle = e^{2r_+}/2$  and  $\langle \hat{p}_{\text{in}}^2 \rangle = e^{-2r_-}/2$  with  $r_+, r_- > 0$ . The ancillary state from OPO-2 is an orthogonally squeezed state with  $\langle \hat{x}_{\text{a}}^2 \rangle = e^{-2r_-}/2$  and  $\langle \hat{p}_{\text{a}}^2 \rangle = e^{2r_+}/2$ . These two fields interfere at the beam splitter having variable transmissivity  $T$  and then they are sent to two homodyne detectors. The homodyne detectors measure the quadrature amplitudes  $\hat{x}_{1,\theta} = \hat{x}_1 \cos \theta + \hat{p}_1 \sin \theta$  and  $\hat{x}_{2,\phi} = \hat{x}_2 \cos \phi + \hat{p}_2 \sin \phi$ . Here  $(\hat{x}_1, \hat{p}_1)$  and  $(\hat{x}_2, \hat{p}_2)$  are the quadrature amplitudes of the upper and lower beams coming out of the variable beam splitter, respectively. The parameters of the processor  $T$ ,  $\theta$ , and  $\phi$  can be varied via the applied voltage to the corresponding electro-optic modulators (EOMs). Then  $\hat{x}_{1,\theta}$  is fed forward to  $\hat{x}_{2,\phi}$  with a certain gain. To let the above-described circuit act as the gate designated by  $(\boldsymbol{\eta}, \boldsymbol{\gamma})$  as Eq. (3), the parameters of the optical circuit are determined by  $T = 1/(1+\gamma^2)$ ,  $\tan \theta = \gamma^2/[\gamma - 2\eta(1+\gamma^2)]$ , and  $\tan \phi = \gamma$ , and correspondingly the feedforward gain is set by  $g = \sqrt{\gamma^2 - 4\eta\gamma + 4\eta^2(1+\gamma^2)}$ , in which settings the contribution of the anti-squeezed quadrature of the ancilla  $\hat{p}_{\text{a}}$  to the gate output is canceled so that the measurement-induced gate operates properly. The constant displacement of  $x_d = 2a\eta\gamma$  is also performed for the constant term in Eq. (3). The feedforward and constant displacing are numerically done by post-processing in the classical computer, which is justified because it gives the same results as those given by optical displacing. In fact, feedforward operations were performed by post-

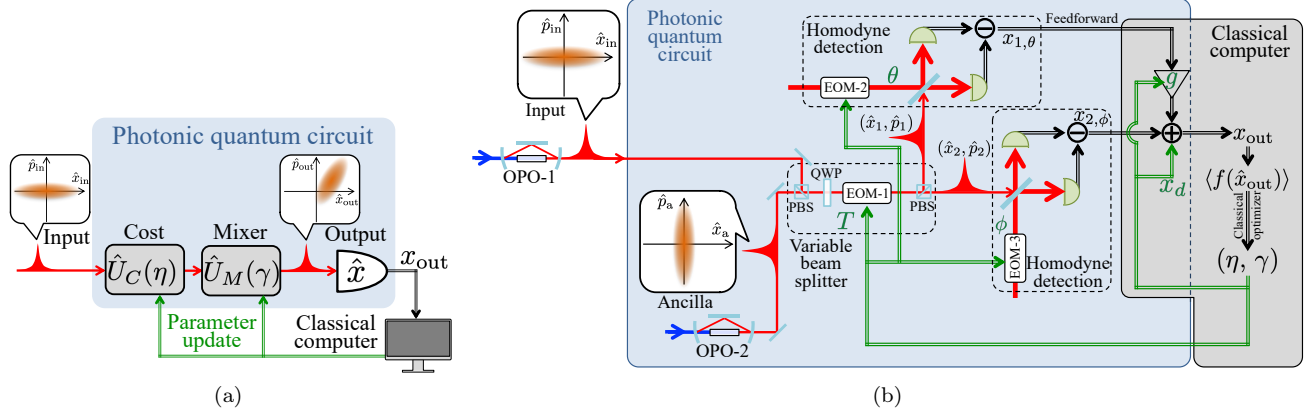


FIG. 1. **Experimental implementation of the CV-QAOA.** **a**, Conceptual diagram of our demonstration. The input state is a squeezed state. The cost operator  $\hat{U}_C(\eta)$  and the mixer operator  $\hat{U}_M(\gamma)$  are applied to it, and the output state is measured in the  $\hat{x}$ -basis. The cost and mixer operators are updated following a certain protocol according to the circuit output  $x_{\text{out}}$ . **b**, Experimental setup. The input state is produced by OPO-1, and the ancillary state for the measurement-induced operation is produced by OPO-2. They interfere at the beam splitter having a variable transmissivity of  $T$ , and each of the two beams from the beam splitter is measured by the homodyne detector with a programmable measurement basis  $\hat{x}_{1,\theta}$  and  $\hat{x}_{2,\phi}$ . The feedforward operation proportional to  $\hat{x}_{1,\theta}$  and the constant displacement operation are applied to  $\hat{x}_{2,\phi}$  in a post process, which yields the circuit output  $x_{\text{out}}$ . The circuit parameters  $(T, \theta, \phi)$ , the feedforward gain  $g$ , and the constant displacement  $x_d$  are determined according to a set of  $(\eta, \gamma)$  so that the measurement-induced gate is performed in a consistent way. EOM, electro-optic modulator; PBS, polarizing beam splitter; QWP, quarter-wave plate.

processing in recent demonstrations of one-way quantum computation<sup>28,29</sup>. After the above classical post-processing, the gate output  $\hat{x}_{\text{out}}$  becomes

$$\hat{x}_{\text{out}} = (1 - 2\eta\gamma)\hat{x}_{\text{in}} + \gamma\hat{p}_{\text{in}} + 2a\eta\gamma - 2\eta\hat{x}_a, \quad (4)$$

which asymptotically coincides with Eq. (3) in the high squeezing limit  $r_- \rightarrow \infty$  in the sense that the variance of the noise term  $-2\eta\hat{x}_a$  approaches zero (see the Supplementary Information for the derivations). Therefore, our photonic processor depicted in Fig. 1b is capable of obtaining the  $x$ -measurement result of the output state,  $\hat{x}_{\text{out}}$ , with the gate parameters  $\eta$  and  $\gamma$  varied.

## OPTIMIZATION LANDSCAPE AND ALGORITHM PERFORMANCE

The CV-QAOA is performed on the processor as follows; first, we repeatedly run the circuit and sample  $\hat{x}_{\text{out}}$  with the parameters  $\eta$  and  $\gamma$  fixed to calculate the mean value  $\langle f(\hat{x}_{\text{out}}) \rangle$ ; then, an outer-loop optimizer in the classical computer suggests new parameters to decrease  $\langle f(\hat{x}_{\text{out}}) \rangle$ . These two stages are repeated alternately. To experimentally demonstrate the capability of the above, we operate the whole system in three different conditions for the parameter update: (i) the parameters  $\eta$  and  $\gamma$  are scanned like a grid search; (ii) the parameters are fixed at their optimum; (iii) the parameters are updated according to the protocol of the Bayesian optimization. Each result is shown in the following.

First, to qualitatively diagnose that the processor operates properly for the full search range of the outer-

loop optimizer,  $\langle f(\hat{x}_{\text{out}}) \rangle$  is evaluated with the parameters  $\eta$  and  $\gamma$  scanned like a grid search. The landscapes of  $\langle f(\hat{x}_{\text{out}}) \rangle$  as a function of  $\eta$  and  $\gamma$  are obtained from the experiment or the numerical simulation as shown in Fig. 2. The landscape structure of the experiment reasonably well agrees with that of the simulation. Specifically,  $\langle f(\hat{x}_{\text{out}}) \rangle$  is small around  $\eta\gamma = 1/2$  and the smallest around  $(\eta, \gamma) = (1/2, 1)$ , which is the theoretical optimum in the high squeezing limit indicated by white stars in the figure. Note that the optimal point in the finite-squeezing case is  $(\eta, \gamma) = (\sqrt{1 - \delta}/2, \sqrt{1 - \delta})$ , where  $\delta = e^{-2r_-}/(e^{2r_+} + 2a^2)$ , and thus the deviation from  $(1/2, 1)$  is less than 2% with the values of  $r_+$  and  $r_-$  for our experiment (see methods) no matter the value of  $a$ . The overall landscape structure is also independent of the value of  $a$  because it only affects the steepness of the valley of  $\eta\gamma \sim 1/2$ .

Next, to visualize how the algorithm works like the gradient descent method to reshape the wavefunction of  $\hat{x}$ , we run the processor with the parameters fixed at the optimal point  $(\eta, \gamma) = (1/2, 1)$ . Figure 3 shows the histogram of the sampled  $\hat{x}_{\text{out}}$  for a specific  $a$ . The sampling results of the input state  $\hat{x}_{\text{in}}$  are also plotted. It can be found that the input state has a broad distribution, and the optimal gate operation localizes the distribution around  $a$ , the exact solution. In fact, the standard deviation of  $\hat{x}_{\text{out}}$  is  $0.5767(4)$ , smaller than that of the vacuum state  $1/\sqrt{2}$  thanks to the quantumness of the processor. Also, the gap between the mean output and the exact solution is  $\langle \hat{x}_{\text{out}} \rangle - a = -7.1(5) \times 10^{-3}$ , the absolute value of which is much smaller than the standard deviation. This indicates that the systematic shift from the

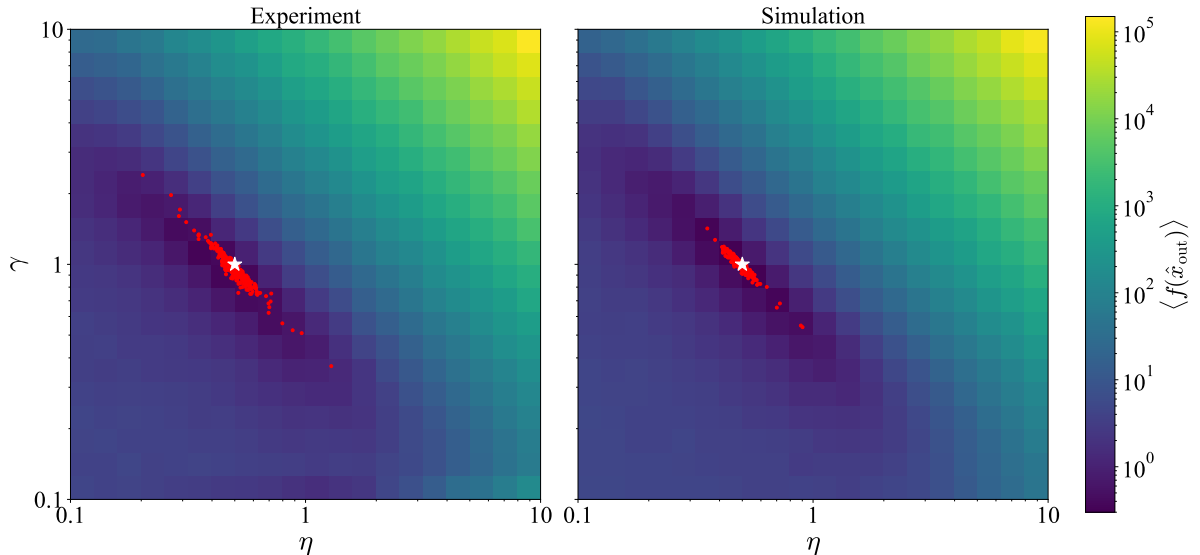


FIG. 2. **Experimental and simulated landscapes of the CV-QAOA.** The landscape structure of the experiment (left) agrees with that of the simulation (right). Each grid is evaluated by 1000 samples of  $\hat{x}_{\text{out}}$ .  $f(x) = (x - 1)^2$  is used for the landscape evaluations. Each red dot on the landscapes shows the parameter set that records the smallest  $\langle f(\hat{x}_{\text{out}}) \rangle$  during the 100-step Bayesian optimization. The white stars denote the theoretical optimum of  $(\eta, \gamma) = (1/2, 1)$ .

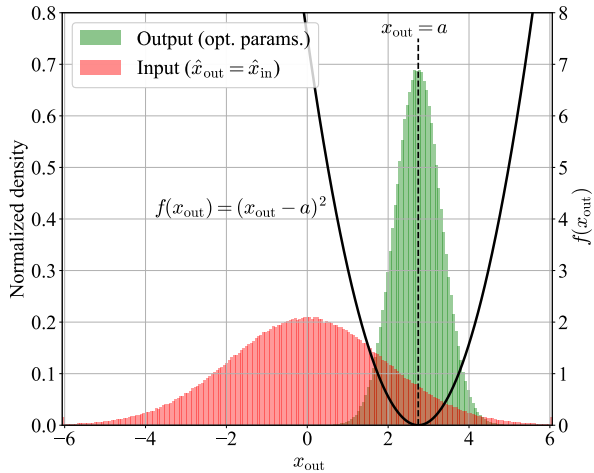
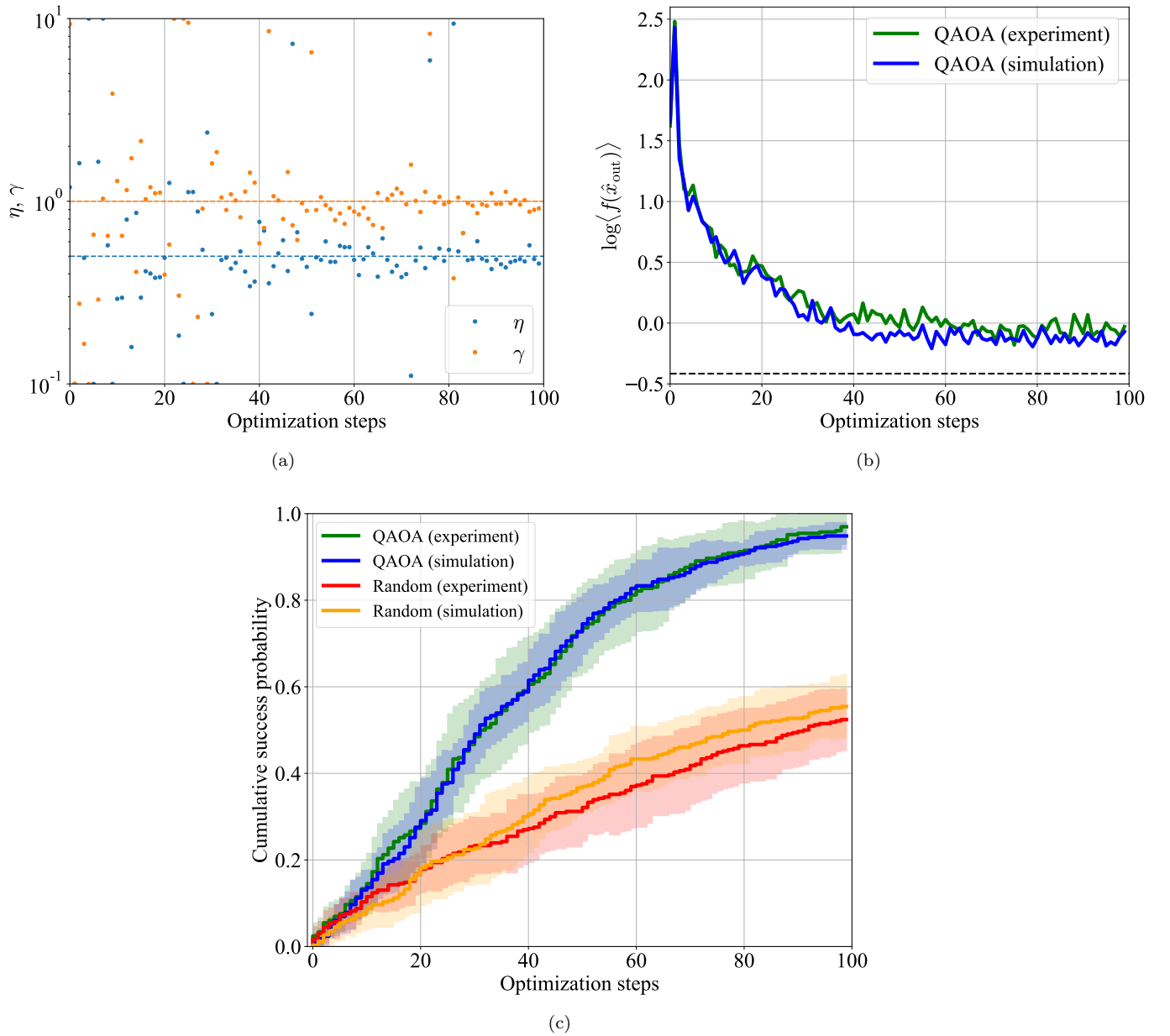


FIG. 3. **Histogram of the output distribution.** The normalized frequencies of the sampled  $x_{\text{out}}$  in the experiment are shown. The green bars are the output distribution with the optimal parameters of  $(\eta, \gamma) = (1/2, 1)$  while the red ones are the distribution of the input state, which corresponds to  $(\eta, \gamma) = (0, 0)$ . The number of the sampled  $x_{\text{out}}$  is  $1.1 \times 10^6$  for each. The curve of  $f(x_{\text{out}}) = (x_{\text{out}} - a)^2$  is overlaid. We use  $a = 2.745$  for these measurements. The comparison of two distributions demonstrates how the CV-QAOA works.

exact solution is negligible with respect to the statistical broadening of the distribution. These results visually prove that the experimentally implemented gate for  $\hat{U}(\eta, \gamma)$  in our problem setting properly localizes the distribution around the minimum like the gradient descent method when the parameters are optimal.

Finally, to evaluate the performance of the CV-QAOA in a realistic condition where the optimum of the parameters is unknown, we perform the algorithm with the parameter updated by the Bayesian optimization. The optimizer suggests new parameters every 1000 samples of  $\hat{x}_{\text{out}}$  so that  $\log\langle f(\hat{x}_{\text{out}}) \rangle$  is minimized (see Methods for more information of the classical optimization). We repeat such a process many times with the value of  $a$  changed to see the statistical behavior of the algorithm. In Fig. 2, the overlaid red dots show the distribution of the classically optimized pair of  $(\eta, \gamma)$ . Each dot corresponds to the pair of the parameters that gives the smallest  $\langle f(\hat{x}_{\text{out}}) \rangle$  among 100 suggestions by the optimizer for each execution of the CV-QAOA. These figures show that the classical optimizer reaches the point around the optimum within the 100 steps as the simulation predicts. Figure 4a shows the typical trace of the parameter update by the Bayesian optimization, where a wide area is initially explored but gradually the search becomes concentrated around the optimum. The behavior of  $\log\langle f(\hat{x}_{\text{out}}) \rangle$ , which is the target function of the Bayesian optimization, is shown in Fig. 4b. The traces denote the average of  $\log\langle f(\hat{x}_{\text{out}}) \rangle$  for all the CV-QAOA trials. The observed decreasing trend of the average of the target function is comparable to the simulation expectation. The small differences between the experimental and simulated traces can be attributed to imperfections of the optical setup such as intensity fluctuations and/or alignment drifts of the local oscillator beams for the homodyne detectors.

To quantify the performance in minimizing the function, the success probability of finding the minimum is evaluated experimentally and numerically. Figure 4c



**FIG. 4. Algorithm performance with parameter updates.** **a**, Typical trace of the parameters updated by the Bayesian optimization. The initial search uniformly spans the full range but gradually the search becomes concentrated around the optimum, which is depicted by the dashed lines. **b**, Convergence of the classical optimization. The solid traces show the average of the target function  $\log\langle f(\hat{x}_{\text{out}}) \rangle$  from the experiment and the simulation. The black dashed line is the theoretical values for the case where the parameters are fixed at  $(\eta, \gamma) = (1/2, 1)$ . **c**, Success probability to sample  $x_{\text{out}}$  such that  $f(x_{\text{out}}) < 1 \times 10^{-9}$ . The solid line is derived by averaging the probability for the eleven sets of such trials. The shaded area shows the  $\pm 1\sigma$  region around the average. The green and blue plots are the experimental and simulated results of the CV-QAOA, respectively. As a reference, the red and orange plots show the experimental and simulated results of random sampling. They indicate that the CV-QAOA finds the minimum of  $f(x)$  significantly more efficiently than the random sampling.

shows the cumulative success probability of finding the minimum of  $f(x)$  up to a certain step of the parameter updates. Here we set the criterion of the success by  $f(x_{\text{out}}) = (x_{\text{out}} - a)^2 < 1 \times 10^{-9}$ . The success probability is calculated by the success frequency for 30 different values of  $a$  in  $f(x) = (x - a)^2$ . The solid line is derived by

averaging the success probability for eleven sets of the trials while the shaded area denotes the  $\pm 1\sigma$ -region around the average derived from the eleven trials. These results show that the experimental results of the increase of the cumulative success probability coincide with the numerically simulated ones. They also show that the success

probability obtained by the CV-QAOA is significantly better than that by random sampling, where the input state is directly measured.

## DISCUSSION

In conclusion, we demonstrate the successful implementation of the CV-QAOA with the parameters of the programmable photonic quantum processor updated. The demonstration experimentally shows that the performance of the algorithm for the minimization of quadratic functions is significantly better than that of the random sampling and comparable to what the numerical simulation predicts. Even though the experimental system is influenced by various noise sources including optical loss, the CV-QAOA still successfully finds the minimum of the function, indicating that the algorithm works robustly. Thus, our results confirm that VQAs have the potential to extract high computational power from a noise-sensitive CV system by taking advantage of its infinite-dimensional nature. Although our implementation is for minimizing quadratic functions, it can be extended to higher-order functions by using proper ancillary states other than squeezed states<sup>33</sup>. It can also be extended to multivariable functions by using multi-mode gates. For such more complex functions, we may set  $P > 1$  with a deeper circuit at the cost of the increased number of the classical parameters to be optimized  $(\eta, \gamma)$ . This work is the first experimental realization of a quantum algorithm using CV information, which proves the usefulness of CV quantum systems for natively solving CV problems. This demonstration sheds light on the advantage of CV quantum computing that its infinite dimensional space can be exploited in NISQ applications. It stimulates the realizations of other VQAs in CV systems such as quantum machine learning<sup>12,13</sup> and thus opens a new promising way toward quantum advantage.

## METHODS

**Classical optimization.** For the update of the circuit parameters  $(\eta, \gamma)$ , we adopt the Bayesian optimization, which has been commonly used among the derivative-free optimization methods in the parameter optimization of the QAOA<sup>6,7</sup>. The following conditions of the Bayesian optimization are set after checking the convergence of the circuit parameters in numerical simulations.  $\log \eta$  and  $\log \gamma$  are handed to the Bayesian optimizer as free parameters. The target function to be optimized is  $\log \langle f(\hat{x}_{\text{out}}) \rangle$ . We use a python package for the Bayesian optimization<sup>34</sup>. The Matérn kernel with  $\nu = 2.5$  is chosen as the covariance kernel function. The acquisition function is a type called the upper confidence bound given by  $\mu + \kappa(t)\sigma$ , where  $\mu$  and  $\sigma$  are the estimated mean and standard deviation of the target function, respectively. We set  $\kappa(t) = \kappa_0 \times 0.97^t$ , where  $\kappa_0 = 2.576$  and  $t$  is the

number of optimization steps.

As for the QAOA of the qubit system, the parameter range of the unitary operations is often limited by  $[0, 2\pi)$ . However, the CV case does not have such a limit. Since it is difficult to optimize parameters with unlimited search range, we limit the range by estimating the order of the optimum of the parameters using a generic prescription (Supplementary Information). The search range of the parameters is set by  $0.1 < \eta < 10$  and  $0.1 < \gamma < 10$  because the optimum is estimated to be  $(\eta_{\text{opt}}, \gamma_{\text{opt}}) \sim (1, 1)$ .

**Repeated execution of the circuits.** In the demonstration of the CV-QAOA with parameters updated (Fig. 4), the iterations of the circuit execution are hierarchical. For clarity, the conditions for that hierarchical execution are summarized here. For each pair of the parameters, we repeatedly run the circuit and sample  $\hat{x}_{\text{out}}$  1000 times with the parameters fixed to obtain  $\langle f(\hat{x}_{\text{out}}) \rangle$ . The Bayesian optimizer suggests 100 pairs of the parameters by using the results of  $\langle f(\hat{x}_{\text{out}}) \rangle$ . Such 100-step classical optimization is repeated eleven times for the same value of  $a$  (in  $f(x) = (x - a)^2$ ). Finally, this repeat is done for 30 different values of  $a$ .

The values of  $a$  are randomly sampled from the Gaussian distribution of zero mean and the standard deviation equal to 1.99, which corresponds to  $\sqrt{\langle \hat{x}_{\text{in}}^2 \rangle}$ . This is because we intend to mimic the following situation. Suppose that the range of  $x$  that gives the minimum of  $f(x)$  ( $x_{\text{min}}$ ) can be roughly estimated by some conditions in the problem settings such as, for example, physical conditions or features of  $f(x)$ . In this case, the distribution of the initial state can be set so that it covers the estimated range for  $x_{\text{min}}$ . In this demonstration, mimicking the situation where the range estimation is correct and the solution  $a$  is in fact in the estimated range, we repeatedly execute the CV-QAOA with many different  $a$  sampled from that range to statistically evaluate the performance of the algorithm. Note that the range for  $x_{\text{min}}$  can always be matched to the range of the initial state distribution by rescaling and translating  $x$ , and resultantly redefining  $f(x)$ . Generally, if the estimation is incorrect, one can perform the algorithm again with an effectively broader initial state.

**Experimental setup.** We use a continuous-wave laser of wavelength 1545.3 nm. Two OPOs are pumped by the second harmonic fields with wavelength of 772.7 nm. The pump power is set to 200 mW. The full width at the half-maximum of the OPOs is 60 MHz. The variable beam splitter is composed of a bulk electro-optic modulator named EOM-1, a quarter-wave plate, and a pair of polarizing beam splitters. EOM-1 serves as a variable polarization rotator and thus works as a variable beam splitter with polarization optics. We inserted the quarter-wave plate so that the transmissivity is 50 % when no voltage is applied to EOM-1, which makes it easy to lock the relative phase between the input and the ancillary beams.

Each homodyne detection is performed by interfering the local oscillator field with the signal field at a 50:50 beam splitter. Two beams from the beam splitter are received by two photodiodes, the photocurrents of which are subtracted with each other and amplified in the electric circuit. The bandwidth of the circuit is about 200 MHz. The optical power of the local oscillator field is set to 10 mW. A fiber-coupled electro-optic modulator shifts the optical phase of each local oscillator for the control of the homodyne angle  $\theta$  or  $\phi$ .

The outcome of the homodyne detection is acquired by an oscilloscope and then sent to the classical computer. The time series from the oscilloscope is converted to a quadrature amplitude by convoluting it with a mode function  $h(t)$  defined by

$$h(t) = \begin{cases} t e^{-\gamma^2 t^2} & (|t| < t_1) \\ 0 & (\text{otherwise}) \end{cases}, \quad (5)$$

where  $\gamma = 3 \times 10^7$  /s and  $t_1 = 50$  ns. The purpose of

using this mode function is to eliminate undesirable effect from low-frequency electrical noise from homodyne detectors<sup>35</sup>. As a preliminary measurement, the outputs of OPO-1 and OPO-2 are measured by the homodyne detectors with the transmissivity of the variable beam splitter set to zero. The squeezing level and the anti-squeezing level of these modes are measured to be  $-5.3$  dB and  $+9.0$  dB on average. This measurement result indicates that the overall optical loss of the experimental setup is estimated to be 22 %.

**Simulation condition.** In the simulation, the optical circuit is numerically simulated by expressing the quadratures of the initial and ancillary states using Gaussian random numbers. Based on the measured squeezing level, we set  $\langle \hat{x}_{\text{in}}^2 \rangle = \langle \hat{p}_{\text{a}}^2 \rangle = 10^{9.0/10}/2$  and  $\langle \hat{p}_{\text{in}}^2 \rangle = \langle \hat{x}_{\text{a}}^2 \rangle = 10^{-5.3/10}/2$ . The asymmetry between the squeezing and anti-squeezing implies that optical loss is taken into account. No other imperfections are included in the simulation.

---

[1] J. Preskill, *Quantum Computing in the NISQ era and beyond*. *Quantum*, **2** 79, (2018).

[2] M. Cerezo *et al.*, *Variational quantum algorithms*. *Nature Reviews Physics*, **3**(9) 625–644, (2021).

[3] E. Farhi, J. Goldstone, and S. Gutmann, *A Quantum Approximate Optimization Algorithm*. arXiv:1411.4028 [quant-ph], (2014).

[4] A. Peruzzo *et al.*, *A variational eigenvalue solver on a photonic quantum processor*. *Nature Communications*, **5**(1) 4213, (2014).

[5] K. Mitarai, M. Negoro, M. Kitagawa, and K. Fujii, *Quantum circuit learning*. *Physical Review A*, **98**(3) 032309, (2018).

[6] J. S. Otterbach *et al.*, *Unsupervised Machine Learning on a Hybrid Quantum Computer*. arXiv:1712.05771 [quant-ph], (2017).

[7] A. Bengtsson *et al.*, *Improved Success Probability with Greater Circuit Depth for the Quantum Approximate Optimization Algorithm*. *Physical Review Applied*, **14**(3) 034010, (2020).

[8] G. Pagano *et al.*, *Quantum approximate optimization of the long-range Ising model with a trapped-ion quantum simulator*. *Proceedings of the National Academy of Sciences*, **117**(41) 25396–25401, (2020).

[9] M. P. Harrigan *et al.*, *Quantum approximate optimization of non-planar graph problems on a planar superconducting processor*. *Nature Physics*, **17**(3) 332–336, (2021).

[10] V. Havlíček *et al.*, *Supervised learning with quantum-enhanced feature spaces*. *Nature*, **567**(7747) 209–212, (2019).

[11] G. Verdon, J. M. Arrazola, K. Brádler, and N. Killoran, *A Quantum Approximate Optimization Algorithm for continuous problems*. arXiv:1902.00409 [quant-ph], (2019).

[12] N. Killoran *et al.*, *Continuous-variable quantum neural networks*. *Physical Review Research*, **1**(3) 033063, (2019).

[13] J. M. Arrazola *et al.*, *Machine learning method for state preparation and gate synthesis on photonic quantum computers*. *Quantum Science and Technology*, **4**(2) 024004, (2019).

[14] T. Volkoff, Z. Holmes, and A. Sornborger, *Universal Compiling and (No-)Free-Lunch Theorems for Continuous-Variable Quantum Learning*. *PRX Quantum*, **2**(4) 040327, (2021).

[15] M. Stéchly, N. Bashige, and P. Chojecki, *Approaching graph problems with continuous variable quantum computing*. arXiv:1906.07047 [quant-ph], (2019).

[16] C. S. Hamilton *et al.*, *Gaussian Boson Sampling*. *Physical Review Letters*, **119**(17) 170501, (2017).

[17] H.-S. Zhong *et al.*, *Phase-Programmable Gaussian Boson Sampling Using Stimulated Squeezed Light*. *Physical Review Letters*, **127**(18) 180502, (2021).

[18] L. S. Madsen *et al.*, *Quantum computational advantage with a programmable photonic processor*. *Nature*, **606**(7912) 75–81, (2022).

[19] J. Huh, G. G. Guerreschi, B. Peropadre, J. R. McClean, and A. Aspuru-Guzik, *Boson sampling for molecular vibronic spectra*. *Nature Photonics*, **9**(9) 615–620, (2015).

[20] J. M. Arrazola and T. R. Bromley, *Using Gaussian Boson Sampling to Find Dense Subgraphs*. *Physical Review Letters*, **121**(3) 030503, (2018).

[21] L. Zhou, S.-T. Wang, S. Choi, H. Pichler, and M. D. Lukin, *Quantum Approximate Optimization Algorithm: Performance, Mechanism, and Implementation on Near-Term Devices*. *Physical Review X*, **10**(2) 021067, (2020).

[22] M. Willsch, D. Willsch, F. Jin, H. De Raedt, and K. Michielsen, *Benchmarking the quantum approximate optimization algorithm*. *Quantum Information Processing*, **19**(7) 197, (2020).

[23] G. Cornuéjols, J. Peña, and R. Tütüncü, *Optimization Methods in Finance*. Cambridge University Press, (2006).

[24] C. C. Aggarwal. *Linear Algebra and Optimization for Machine Learning*. Springer International Publishing,

Cham, (2020).

[25] S. S. Rao. *Engineering Optimization : Theory and Practice*. John Wiley & Sons, (1996).

[26] A. K. Pati, S. L. Braunstein, and S. Lloyd, *Quantum searching with continuous variables*. arXiv:quant-ph/0002082, (2000).

[27] K. Fukui and S. Takeda, *Building a large-scale quantum computer with continuous-variable optical technologies*. Journal of Physics B, **55**(1) 012001, (2022).

[28] W. Asavanant *et al.*, *Time-Domain-Multiplexed Measurement-Based Quantum Operations with 25-MHz Clock Frequency*. Physical Review Applied, **16**(3) 034005, (2021).

[29] M. V. Larsen, X. Guo, C. R. Breum, J. S. Neergaard-Nielsen, and U. L. Andersen, *Deterministic multi-mode gates on a scalable photonic quantum computing platform*. Nature Physics, **17**(9) 1018–1023, (2021).

[30] Y. Enomoto, K. Yonezu, Y. Mitsuhashi, K. Takase, and S. Takeda, *Programmable and sequential Gaussian gates in a loop-based single-mode photonic quantum processor*. Science Advances, **7**(46) eabj6624, (2021).

[31] R. Filip, P. Marek, and U. L. Andersen, *Measurement-induced continuous-variable quantum interactions*. Physical Review A, **71**(4) 042308, (2005).

[32] K. Miyata *et al.*, *Experimental realization of a dynamic squeezing gate*. Physical Review A, **90**(6) 060302, (2014).

[33] P. Marek *et al.*, *General implementation of arbitrary nonlinear quadrature phase gates*. Physical Review A, **97**(2) 022329, (2018).

[34] F. Nogueira, *bayesian-optimization*. <https://github.com/fmfn/BayesianOptimization>, (2014).

[35] J. Yoshikawa *et al.*, *Invited Article: Generation of one-million-mode continuous-variable cluster state by unlimited time-domain multiplexing*. APL Photonics, **1**(6)

060801, (2016).

## ACKNOWLEDGMENTS

This work was partly supported by JSPS KAKENHI Grant Numbers 20H01833 and 21K18593, MEXT Leading Initiative for Excellent Young Researchers, Toray Science Foundation (19-6006), and the Canon Foundation. The authors thank Keisuke Fujii, Kosuke Fukui, and Kosuke Mitarai for valuable discussions. The authors also thank Takahiro Mitani for the careful proof-reading of the manuscript.

## AUTHOR CONTRIBUTIONS

Y. E. contributed to the development of the optical and electrical part of the experimental setup. Y. E. and K. A. contributed to the adjustment, tuning, and debugging of the experimental setup, the data acquisition and analysis, and the numerical simulation. K. U. contributed to the development of the optical setup, in particular for the optical parametric oscillators and the homodyne detections. S. T. conceived, planned, and designed the whole system, supervising the project. All authors contributed to writing the manuscript.

## COMPETING INTERESTS

The authors declare no competing interests.

## Supplementary Information:

## Continuous-variable quantum approximate optimization on a programmable photonic quantum processor

Yutaro Enomoto,\* Keitaro Anai, Kenta Udagawa, and Shuntaro Takeda†

Department of Applied Physics, School of Engineering, The University of Tokyo,  
7-3-1 Hongo, Bunkyo-ku, Tokyo 113-8656, Japan

(Dated: June 16, 2022)

## INPUT-OUTPUT RELATION OF THE OPTICAL CIRCUIT

Let us describe why the optical circuit in Fig. 1b works as the unitary operation  $\hat{U}(\eta, \gamma) = e^{-i\gamma\hat{p}^2/2}e^{-i\eta(\hat{x}-a)^2}$  for our problem setting and the successive measurement in  $\hat{x}$ -basis. Here we recall that this unitary transforms the input state represented by  $(\hat{x}_{\text{in}}, \hat{p}_{\text{in}})$  into the output state represented by  $(\hat{x}_{\text{out}}, \hat{p}_{\text{out}})$  as

$$\begin{bmatrix} \hat{x}_{\text{out}} \\ \hat{p}_{\text{out}} \end{bmatrix} = \begin{bmatrix} 1 - 2\eta\gamma & \gamma \\ -2\eta & 1 \end{bmatrix} \begin{bmatrix} \hat{x}_{\text{in}} \\ \hat{p}_{\text{in}} \end{bmatrix} + \begin{bmatrix} 2a\eta\gamma \\ 2a\eta \end{bmatrix}. \quad (\text{S.1})$$

One of the possible implementations of such a linear transformation is shown in Fig. S1, which is based on the squeezing gate in Ref. [1]. First, we explain how this measurement-induced implementation works. The ancillary state represented by  $(\hat{x}_{\text{a}}, \hat{p}_{\text{a}})$  is an  $x$ -squeezed state. The output of this circuit is calculated as

$$\begin{bmatrix} \hat{x}_{\text{out}} \\ \hat{p}_{\text{out}} \end{bmatrix} = \begin{bmatrix} \cos\phi & \sin\phi \\ -\sin\phi & \cos\phi \end{bmatrix} \begin{bmatrix} \hat{x}_2 \\ \hat{p}_2 + g'\hat{x}_{1,\theta} + x'_d \end{bmatrix} \quad (\text{S.2})$$

$$= \begin{bmatrix} \hat{x}_{2,\phi} + g'\hat{x}_{1,\theta} \sin\phi + x'_d \sin\phi \\ \hat{p}_{2,\phi} + g'\hat{x}_{1,\theta} \cos\phi + x'_d \cos\phi \end{bmatrix}, \quad (\text{S.3})$$

where  $g'$  is the feedforward gain and  $x'_d$  is the constant displacing. Here,  $(\hat{x}_i, \hat{p}_i)$  and  $(\hat{x}_{i,\psi}, \hat{p}_{i,\psi})$  ( $i = 1, 2$ , and  $\psi \in \mathbb{R}$ ) denote the quadrature amplitudes of the beams coming out of the beam splitter defined by

$$\hat{x}_1 = \sqrt{1-T}\hat{x}_{\text{in}} + \sqrt{T}\hat{x}_{\text{a}}, \quad (\text{S.4})$$

$$\hat{p}_1 = \sqrt{1-T}\hat{p}_{\text{in}} + \sqrt{T}\hat{p}_{\text{a}}, \quad (\text{S.5})$$

$$\hat{x}_2 = \sqrt{T}\hat{x}_{\text{in}} - \sqrt{1-T}\hat{x}_{\text{a}}, \quad (\text{S.6})$$

$$\hat{p}_2 = \sqrt{T}\hat{p}_{\text{in}} - \sqrt{1-T}\hat{p}_{\text{a}}, \quad (\text{S.7})$$

$$\begin{bmatrix} \hat{x}_{i,\psi} \\ \hat{p}_{i,\psi} \end{bmatrix} = \begin{bmatrix} \cos\psi & \sin\psi \\ -\sin\psi & \cos\psi \end{bmatrix} \begin{bmatrix} \hat{x}_i \\ \hat{p}_i \end{bmatrix}. \quad (\text{S.8})$$

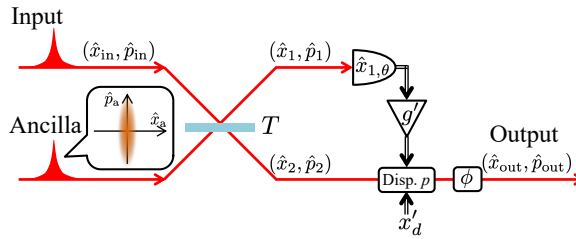


FIG. S1. Optical circuit for a measurement-induced linear transformation. The input state interferes with the ancilla at the beamsplitter having the transmissivity of  $T$ . One outgoing beam from the beamsplitter is measured by homodyne detection, and the measurement outcome is fed forward to the other beam. The quadrature  $\hat{p}_2$  is displaced by  $g'\hat{x}_{1,\theta} + x'_d$ , and then a phase rotation by  $\phi$  is applied.

\* [yenomoto@ap.t.u-tokyo.ac.jp](mailto:yenomoto@ap.t.u-tokyo.ac.jp)† [takeda@ap.t.u-tokyo.ac.jp](mailto:takeda@ap.t.u-tokyo.ac.jp)

If we set the feedforward gain by  $g' = \sqrt{(1-T)/T} / \sin \theta$ , the output described by Eq. (S.3) becomes

$$\begin{bmatrix} \hat{x}_{\text{out}} \\ \hat{p}_{\text{out}} \end{bmatrix} = \frac{1}{\sqrt{T}} \begin{bmatrix} (1-T) \cot \theta \sin \phi + T \cos \phi & \sin \phi \\ (1-T) \cot \theta \cos \phi - T \sin \phi & \cos \phi \end{bmatrix} \begin{bmatrix} \hat{x}_{\text{in}} \\ \hat{p}_{\text{in}} \end{bmatrix} + \begin{bmatrix} \sin \phi \\ \cos \phi \end{bmatrix} x'_d + \sqrt{1-T} \begin{bmatrix} \cot \theta \sin \phi - \cos \phi \\ \cot \theta \cos \phi + \sin \phi \end{bmatrix} \hat{x}_{\text{a}}. \quad (\text{S.9})$$

Note that  $g'$  is chosen so that the anti-squeezed quadrature  $\hat{p}_{\text{a}}$  disappears in this expression. This expression indicates that, apart from a noise term proportional to the squeezed quadrature  $\hat{x}_{\text{a}}$ , the circuit in Fig. S1 is capable of performing various linear transformations by changing  $T$ ,  $\theta$ ,  $\phi$ , and  $x'_d$ . In fact, by setting  $T = 1/(1+\gamma^2)$ ,  $\tan \theta = \gamma^2/[\gamma - 2\eta(1+\gamma^2)]$  ( $0 \leq \theta < \pi$ ),  $\tan \phi = \gamma$  ( $0 \leq \phi < \pi/2$ ), and  $x'_d = 2a\eta\sqrt{1+\gamma^2}$ , Eq. (S.9) becomes

$$\begin{bmatrix} \hat{x}_{\text{out}} \\ \hat{p}_{\text{out}} \end{bmatrix} = \begin{bmatrix} 1 - 2\eta\gamma & \gamma \\ -2\eta & 1 \end{bmatrix} \begin{bmatrix} \hat{x}_{\text{in}} \\ \hat{p}_{\text{in}} \end{bmatrix} + \begin{bmatrix} 2a\eta\gamma \\ 2a\eta \end{bmatrix} + \begin{bmatrix} -2\eta \\ (\gamma - 2\eta)/\gamma \end{bmatrix} \hat{x}_{\text{a}}, \quad (\text{S.10})$$

which asymptotically coincides with Eq. (S.1) in the high squeezing limit of  $\hat{x}_{\text{a}} \rightarrow 0$ . Note that the upper row of this equation is identical to Eq. (4).

Given that we eventually measure the quadrature amplitude  $\hat{x}_{\text{out}}$ , the phase rotation by  $\phi$  can be achieved instead by changing the homodyne angle for the measurement of the output state. In addition, the displacing operation can be replaced by numerical post-processing after the homodyne measurement as the displacing operation only shifts the mean value of the measurement outcome. For this reason, the circuit in Fig. 1b is equivalent to the one in Fig. S1 as long as the quadrature amplitude of the output state is measured. In the circuit in Fig. 1b,  $\hat{x}_{\text{out}}$  is in fact provided using the two homodyne-measurement outcomes by  $\hat{x}_{2,\phi} + g\hat{x}_{1,\theta} + x_d$ , which corresponds to the upper row of Eq. (S.3). Here we redefined  $g := g' \sin \phi = \sqrt{\gamma^2 - 4\eta\gamma + 4\eta^2(1+\gamma^2)}$  and  $x_d := x'_d \sin \phi = 2a\eta\gamma$ .

## PARAMETER SEARCH RANGE OF THE BAYESIAN OPTIMIZATION

To limit the search range of the parameters  $(\eta, \gamma)$  in the Bayesian optimization process, the order of magnitude of the optimal parameters can be estimated in advance if some prior information on the function to be optimized,  $f(x)$ , is available. Here we explain a prescription for the estimation. Let us consider the CV-QAOA with  $P = 1$  for a one-variable function  $f(x)$ . If implemented by a combination of measurement-induced gates [2], a pair of the cost and mixer operations transforms the quadratures as

$$\hat{x}_{\text{out}} = \hat{x}_{\text{in}} + \gamma \hat{p}_{\text{in}} - \eta \gamma \nabla f(\hat{x}_{\text{in}}) + N(\eta, \gamma; \hat{x}_{\text{a}}, \hat{p}_{\text{a}}), \quad (\text{S.11})$$

where  $N$  is a noise term arising from non-ideal ancillary states.  $\hat{x}_{\text{a}}$  and  $\hat{p}_{\text{a}}$  formally denote the quadrature amplitudes of the ancillary states. Let us assume that the ancillary states are linearly or non-linearly squeezed sufficiently and thus  $|\langle N \rangle| \ll |x_{\text{min}}|$ , where  $x_{\text{min}} = \text{argmin} f(x)$ . We can also assume that the optimal parameters, namely  $(\eta_{\text{opt}}, \gamma_{\text{opt}})$ , localize the distribution of  $\hat{x}_{\text{out}}$  around  $x_{\text{min}}$ , and thus provide two conditions:  $\langle \hat{x}_{\text{out}} \rangle \sim x_{\text{min}}$  and  $\langle \Delta \hat{x}_{\text{out}}^2 \rangle$  is minimized. By assuming that the optimal parameters  $(\eta_{\text{opt}}, \gamma_{\text{opt}})$  are adopted and taking the expectation value of Eq. (S.11), the assumption  $\langle \hat{x}_{\text{out}} \rangle \sim x_{\text{min}}$  reduces to

$$\eta_{\text{opt}} \gamma_{\text{opt}} \sim -\frac{x_{\text{min}}}{\langle \nabla f(\hat{x}_{\text{in}}) \rangle}. \quad (\text{S.12})$$

Here we assume  $\langle \hat{x}_{\text{in}} \rangle = 0$  and  $\langle \hat{p}_{\text{in}} \rangle = 0$  since the input state is the squeezed vacuum. In this way, if the prior information on the order of magnitude of  $x_{\text{min}}$  and  $\langle \nabla f(\hat{x}_{\text{in}}) \rangle$  is available, the product  $\eta_{\text{opt}} \gamma_{\text{opt}}$  can be inferred. Let us next consider the variance of  $\hat{x}_{\text{out}}$ . Since Eq. (S.12) estimates the product of the optimal parameters, we evaluate the variance under the constraint of  $\eta\gamma = c$ , where  $c$  denotes the estimated value of the product  $\eta_{\text{opt}} \gamma_{\text{opt}}$ . By substituting  $\eta\gamma = c$  into Eq. (S.11) to eliminate  $\eta$ , we have

$$\langle \Delta \hat{x}_{\text{out}}^2 \rangle \sim \left\langle \Delta [\hat{x}_{\text{in}} - c \nabla f(\hat{x}_{\text{in}})]^2 \right\rangle + \gamma^2 \langle \hat{p}_{\text{in}}^2 \rangle + \left\langle \Delta N^2 \left( \frac{c}{\gamma}, \gamma; \hat{x}_{\text{a}}, \hat{p}_{\text{a}} \right) \right\rangle. \quad (\text{S.13})$$

As the first term does not depend on  $\gamma$ ,  $\gamma_{\text{opt}}$  can be estimated by minimizing the sum of the second and third terms. The third term can be calculated if the specific form of  $N(\eta, \gamma; \hat{x}_{\text{a}}, \hat{p}_{\text{a}})$  is known. Once the third term is calculated, the sum of the second and third terms becomes a one-variable function of  $\gamma$ , which should be able to be minimized.

Let us consider the specific case of  $f(x) = (x - a)^2$ , and estimate the order of magnitude of the optimal parameters by using the typical magnitude of  $\hat{x}_{\text{in}}$ . We denote  $\sqrt{\langle \hat{x}_{\text{in}}^2 \rangle} = \sigma$ , which we regard as the typical magnitude of  $\hat{x}_{\text{in}}$ . As the function  $f(x)$  is quadratic in  $x$  and its leading term is  $x^2$ , the order of magnitude of the variation of  $f(x)$  in the

range of  $\pm\sigma$  can be estimated by  $\sigma^2$ . We then estimate the gradient of the function by dividing the typical range of the function output  $\sigma^2$  by the typical range of the function input  $\sigma$ :  $|\langle \nabla f(x) \rangle| \sim \sigma^2/\sigma = \sigma$ . We can also assume that  $|x_{\min}| \sim \sigma$ . Using these estimations, we can estimate  $\eta_{\text{opt}}\gamma_{\text{opt}}$  as

$$\eta_{\text{opt}}\gamma_{\text{opt}} \sim 1 \quad (\text{S.14})$$

from Eq. (S.12). Let us then calculate the variance under  $\eta\gamma = 1$ . Since  $N(\eta, \gamma; \hat{x}_a, \hat{p}_a) = -2\eta\hat{x}_a$  from Eq. (4), the sum of the second and third terms of Eq. (S.13) becomes  $\gamma^2\langle \hat{p}_{\text{in}}^2 \rangle + (4/\gamma^2)\langle \hat{x}_a^2 \rangle$ . By minimizing this in terms of  $\gamma$ ,  $\gamma_{\text{opt}}$  can be estimated as

$$\gamma_{\text{opt}} \sim (4\langle \hat{x}_a^2 \rangle / \langle \hat{p}_{\text{in}}^2 \rangle)^{1/4} = \sqrt{2} \sim 1. \quad (\text{S.15})$$

In this way, the optimal parameters are estimated as  $(\eta_{\text{opt}}, \gamma_{\text{opt}}) \sim (1, 1)$ , which is why we set the search range by  $[0.1, 10]^{2}$  with a margin of about a factor of ten.

The above discussion is only a rough estimation of the order of magnitude, and although it works in our case, there is no guarantee that the optimal parameters exist in the search range. For this reason, a general strategy may be to perform the CV-QAOA within the initial search range and, if there seems to be the optimal point outside the search range, expand or change the search range by observing the behavior of the parameter optimization.

---

[1] K. Miyata *et al.*, *Experimental realization of a dynamic squeezing gate*. Physical Review A, **90**(6) 060302, (2014).  
[2] P. Marek *et al.*, *General implementation of arbitrary nonlinear quadrature phase gates*. Physical Review A, **97**(2) 022329, (2018).